

PREPRINT

Author-formatted, not peer-reviewed document posted on 09/02/2026

DOI: <https://doi.org/10.3897/arphapreprints.e188103>

The Anatomy of a Mamenchisaurid Tooth Informed by Digital Reconstruction

Sui Zixian, Shao shuai, Yin Yalei

1 The Anatomy of a Mamenchisaurid Tooth Informed by Digital 2 Reconstruction

3 Zi-Xian Sui[†], Shuai Shao^{1†}, Ya-Lei Yin^{1,2,3,4*}

4 1 *College of Paleontology, Shenyang Normal University, Shenyang 110034, China*

5 2 *Observation and Research Station of Stratigraphy, Paleontology and Environmental Geology in
6 Chaohu, MNR, No.999 Xianlonghu Road, Hefei 230001, China*

7 3 *Key Laboratory of Stratigraphy and Paleontology of the Ministry of Natural Resources, Beijing
8 100044, China*

9 4 *Center for Vertebrate Evolutionary Biology, School of Life Sciences, Yunnan University, Kunming
10 650500, China*

11 † *Zi-Xian Sui and Shuai Shao have contributed equally to this work.*

12
13 Corresponding author: Ya-Lei Yin (yinyalei@synu.edu.cn)

15 Abstract

16 The detailed dental anatomy of sauropod mamenchisaurids remains largely unexplored. Here,
17 we describe a well-preserved isolated sauropod tooth from the Upper Jurassic Qigu Formation of
18 the Turpan-Hami Basin, Xinjiang, using high-resolution Micro-CT and three-dimensional
19 reconstruction to investigate its internal anatomy. This tooth exhibits a diagnostic feature of
20 Mamenchisauridae, specifically the presence of marginal denticles restricted to the mesial margin.
21 CT scan data provide novel insights into mamenchisaurid dental anatomy and present the first
22 three-dimensional enamel distribution in sauropod teeth. The lingual ridge forms from thickened
23 enamel and dentine, whereas the lingual boss arises solely from dentine expansion. A labiolingual
24 enamel thickness asymmetry appears in the apical region, convergent with certain neosauropods.
25 The pulp cavity shows a distinct volumetric transition, expanding basally into a bulbous root canal
26 and appearing as a labiolingually compressed lamina structure in the crown. Taxonomic
27 comparison indicates that this tooth represents a mamenchisaurid lineage distinct from the
28 previously only known sauropod tooth from the Qigu Formation. Our study supports diverse
29 sauropod assemblages in the Qigu Formation and provides new anatomical evidence for
30 understanding sauropod dental evolution.

32 Keywords

33 Sauropoda, Late Jurassic, Qigu Formation, Turpan-Hami Basin, Micro-CT, enamel asymmetry,
34 pulp cavity

36 Introduction

37 The family Mamenchisauridae represents a dominant eusauropod clade primarily distributed in
38 the Middl-Late Jurassic of East Asia (Upchurch et al. 2004; Ren et al. 2020, 2021; Moore et al.

2020, 2023). Although most remains have been discovered in China (Ren et al. 2025), fossil evidence indicates their geographic range extended northward to West Siberia (Averianov et al. 2019) and southward to Thailand (Suteethorn et al. 2013), with a potential occurrence also reported from Tanzania in East Africa (Mannion et al. 2019). Mamenchisaurids are notably characterized by pronounced morphological specializations, including extreme neck elongation and gigantism (Moore et al. 2023; Wei et al. 2025). The clade currently comprises at least 18 taxa, although the definition of mamenchisaurid remains controversial (Moore et al. 2023; Dai et al. 2025).

In contrast to their osteology, the dental anatomy of mamenchisaurids, particularly the internal structure of the teeth, remains poorly understood due to limited preservation (Maisch and Matzke 2019a). Current knowledge of mamenchisaurid teeth is based primarily on descriptions of external features in several key taxa, such as *Mamenchisaurus youngi* (Pi et al. 1996; Ouyang and Ye 2002), *M. sinocanadorum* (Russell and Zheng 1993; Moore et al. 2023), *M. jingyanensis* (Zhang et al. 1998), and *M. hochuanensis* (Ye et al. 2001), as well as some isolated teeth from Thailand (Suteethorn et al. 2013) and Russia (Averianov et al. 2019). Nevertheless, some dental features may hold taxonomically importance within Mamenchisauridae. For example, the absence or nearly absence of denticles on the distal margin of the tooth is regarded as a synapomorphy of the clade (Xing et al. 2015; Xu et al. 2021). Additionally, *M. sinocanadorum* distinctly features a parallel-sided tooth crown in labial or lingual view and the presence of a distolingual boss on some dentary teeth (Moore et al. 2023).

The Upper Jurassic Qigu Formation in the Junggar and Turpan-Hami Basins of Xinjiang, has produced a diverse assemblage of vertebrate fossils, such as mammals, turtles, and dinosaurs (Matzke et al. 2005; Pfretzschner et al. 2005; Martin et al. 2010a, 2010b; Wings et al. 2007, 2012, 2015; Rabi et al. 2013; Wu et al. 2013; Maisch and Matzke 2019a, 2019b, 2020; Augustin et al. 2020). Among these, dinosaur remains are scarce. To date, isolated teeth attributed to theropods, sauropods, and stegosaurs, as well as fragmentary bones from stegosaurs and ankylosaurs, have been documented from the Qigu Formation in the Junggar Basin (Wings et al. 2007, 2015; Maisch and Matzke 2019a, 2019b, 2020; Augustin et al. 2020). In contrast, the Qigu Formation of the Turpan-Hami Basin has yielded only the mamenchisaurid *Xinjiangtitan shanshanensis* (Wu et al. 2013; Zhang et al. 2020), with no reported dinosaur teeth to date. Significantly, the sauropod tooth from the Qigu Formation has been provisionally attributed to either ?Mamenchisauridae or a basal representative of Euhelopodidae, given that it lacks unequivocal synapomorphic characteristics that are diagnostic of these clades.

This study reports the discovery of a well-preserved, isolated mamenchisaurid tooth (PMOL-ADt0009) from the Qigu Formation in the Qiketai area of the Turpan-Hami Basin. This finding represents the first documented occurrence of sauropod teeth within the Qigu Formation in this region. To reveal the internal anatomy of the tooth, including the morphology of the pulp cavity and the enamel distribution patterns on the labial and lingual sides, X-ray computed tomography (CT) and three-dimensional reconstruction techniques were employed. By integrating internal and external morphology, this study aims to provide novel insights into the dental anatomy of mamenchisaurids.

Geological Setting

84 The specimen was collected from the same locality and stratigraphic horizon as the
85 mamenchisaurid *Xinjiangtitan shanshanesis* (Wu et al. 2013; Zhang et al. 2020). The fossil locality
86 is situated approximately 8 km south of Qiketai Town, Shanshan County, Xinjiang Uygur
87 Autonomous Region, Northwest China (Fig. 1). The fossil horizon is the Qigu Formation of the
88 Turpan-Hami Basin. Magnetostratigraphic and biostratigraphic studies constrain the geological age
89 of the Qigu Formation to the Late Jurassic (Oxfordian to Kimmeridgian), with the top of the
90 formation dated to approximately 155.3 Ma (Deng et al. 2015). The Qigu Formation lies
91 conformably above the Qiketai Formation and is conformably overlain by the Kalaza Formation
92 (XBGMR 1993).

94 Lithologically, the Qigu Formation consists primarily of purplish-red and brownish-red
95 mudstones and siltstones, intercalated with greyish-green silty mudstones, fine-to medium-grained
96 sandstones, and occasional layers of pebbly sandstone, gypsum veins, and thin-bedded marl (Song
97 et al. 2014). The Qigu Formation in the Turpan-Hami Basin represents a sequence of fluvial-
98 lacustrine deposits formed under semi-arid conditions (Li et al. 2021). In the Qiketai area, the
99 formation can be subdivided into upper, middle, and lower members (Song et al. 2014). Among
100 these, the middle member is the most fossiliferous, yielding abundant vertebrate remains (including
101 sauropods and turtles) as well as bivalve fossils (Song et al. 2014), including the tooth in this study.

103 Material and methods

104 The specimen (PMOL-ADt0009) described in this study is a well-preserved, isolated sauropod
105 tooth discovered in the Gobi Desert, located approximately 8 km south of Qiketai Town, Shanshan
106 County, Xinjiang Uygur Autonomous Region, China. The GPS coordinates of the fossil locality
107 are 42°57.78'N; 90°34.44'E (DDM). Stratigraphically, the specimen was collected from the Upper
108 Jurassic Qigu Formation. It is currently housed in the Paleontological Museum of Liaoning
109 (PMOL), Shenyang, China. The specimen was mechanically prepared using a steel needle under a
110 stereomicroscope to remove the attached matrix. To examine fine dental structures, including
111 marginal denticles and enamel ornamentation, at high resolution, microscopic imaging was
112 performed using an Olympus DSX1000 digital microscope.

114 To non-destructively reveal internal anatomical features, PMOL-ADt0009 underwent high-
115 resolution X-ray computed tomography (CT) scanning at the Laboratory of Stratigraphy and
116 Paleontology, Institute of Geology, Chinese Academy of Geological Sciences (IG-CAGS), Beijing,
117 China, using a Nikon XT H 225 ST scanner. A total of 3141 projections were generated at an
118 operating voltage of 110 kV and a current of 115 μ A. The reconstructed voxel size was $26.41 \times$
119 $26.41 \times 26.41 \mu\text{m}$. Three-dimensional reconstruction, morphometric measurements, volume
120 calculation and enamel wall thickness analysis (using the sphere method) were performed with VG
121 STUDIO MAX 3.4.0 software (Volume Graphics, Heidelberg, Germany).

123 The slenderness index (SI) is calculated as the ratio of crown height to the maximum mesiodistal
124 crown width (Upchurch 1998). The compression index (CI) is defined as the ratio between the
125 maximum labiolingual crown diameter and the maximum mesiodistal crown diameter (Díez Díaz
126 et al. 2013; Bindellini and Dal Sasso 2021). The expansion index is the ratio of the maximum
127 mesiodistal widths of tooth crowns to their basal breadths (Moore et al. 2023). The determination

128 of labiolingual and mesiodistal orientations in isolated teeth is based on the asymmetry of the tooth
129 morphology. This includes features such as the D-shaped cross-section and the position of the apex
130 of the 'D' situated close to the mesial margins (Canudo et al. 2002; Barrett and Wang 2007; Amiot
131 et al. 2010).

132

133 Systematic Paleontology

134

135 **Dinosauria Owen, 1842**

136 **Sauropoda Marsh, 1878**

137 **Mamenchisauridae Young and Zhao, 1972**

138 **Mamenchisauridae indet.**

139

140 Description

141 **General.** The specimen (PMOL-ADt0009) is preserved as an isolated tooth, retaining a relatively
142 complete crown and the basal portion of the root (Fig. 2). It has a SI of 2.03 and a CI of 0.80 (Table
143 1). The presence of mesial and distal facets, along with a distinct apical wear facet, collectively
144 demonstrates that it was a functional tooth. PMOL-ADt0009 is generally characterized as a
145 spatulate tooth. Notably, the cervix extends more basally on the lingual side than on the labial side
146 (Fig. 2A–H).

147

148 **Crown.** The crown curves lingually. The crown apex is positioned distally (Fig. 2C, D). The
149 crown exhibits a characteristic D-shaped cross-section at its apical half, attributable to the strongly
150 convex labial surface and the concave lingual surface (Fig. 2). The apex of the 'D' shape is
151 positioned more mesially, with the portion of the crown mesial to the apex exhibiting greater
152 convexity compared to the distal section. The labial surface is gently convex apicobasally (Fig. 2E–
153 H). The mesial and distal margins of the crown are evenly spaced along the basal two-thirds and
154 gradually converge toward the apex along the apical one-third (Fig. 2C, D). The crown's expansion
155 index is $\leq 120\%$ (Table 1), with parallel sides in the labial view. The enamel, dentine, and pulp
156 cavity of the crown were segmented. The total volumes of the enamel, dentine, and pulp cavity
157 were measured as 415.87 mm^3 , 2852.11 mm^3 , and 73.12 mm^3 , respectively. It is noteworthy that
158 the pulp cavity exhibited the smallest volume among the three structural components of the crown.

159

160 Three wear facets are present. The apical wear facet is nearly circular in shape, oriented lingually,
161 and inclined at approximately 25 degrees relative to the long axis of the crown. Two lateral wear
162 facets exhibit a V-shaped morphology and are located along the mesial and distal margins of the
163 crown. These lateral facets are subequal in apicobasal length. The mesial facet consistently faces
164 linguoapically, whereas the distal facet is oriented linguodistally (Fig. 2C, D). The mesial facet is
165 well-developed, in contrast to the distal facet, which is at an early stage of attrition. The mesial
166 facet is confluent with the apical wear facet, while the distal facet appears to be separate from the
167 apical wear facet (Fig. 2C, D). Furthermore, the mesial wear facet progressively narrows
168 mesiobasally (Fig. 2C, D), whereas the distal wear facet extends linearly along the distal margin.

169

170 Specifically, distinct marginal denticles are observed and primarily restricted to the apical one-
171 fifth of the crown along the mesial margin (Fig. 3A). In total, eight denticles have been identified
172 and numbered sequentially from 1 to 8. The first three denticles, located on the mesial wear facet,
173 have been worn away, leaving circular concavities (Fig. 3B). Their diameters are approximately
174 0.65 mm. The fourth denticle exhibits partial damage. Conversely, the remaining four denticles are
175 well-preserved, characterized by a blunt or coarsely granular morphology, and are clearly
176 demarcated from one another (Fig. 3B).

177
178 On the labial surface, a distinct apicobasal groove is present near the distal margin, extending
179 apicobasally along the crown and gradually diminishing towards the apex (Fig. 2A, B). Distal to
180 this groove, a distinct, flattened surface is delineated along the distolabial margin (Fig. 2B, H),
181 extending basally from the cervix and apically to the point of maximum mesiodistal width. The
182 enamel on the labial surface displays a distinct rugose texture, characterized by fine, densely
183 packed wrinkles extending from the base to near the apex (Fig. 2A, B). The ornamentation of this
184 specimen consists of closely spaced, sub-parallel, and interwoven crests and grooves oriented along
185 the apicobasal axis (Fig. 2B). This wrinkled texture gradually smooths towards the apex (Fig. 2A,
186 B), likely as a result of antemortem wear. A distinct area of enamel spalling is present on the
187 mesiolabial aspect of the crown apex, exposing the underlying dentine (Fig. 2A, B, E, F, I, J), which
188 is attributed to tooth-to-tooth occlusion.

189
190 The lingual surface is generally concave, exhibiting the characteristic shovel-like morphology
191 typical of spatulate teeth (Fig. 2C, D). Enamel spalling is observed on the lingual surface in certain
192 areas, notably on the distobasal portion of the crown, where the dentine is completely exposed (Fig.
193 2G, H). Enamel wrinkles are also present on the lingual surface, although they are poorly preserved
194 (Fig. 2C, D). The lingual surface is divided into two asymmetrical longitudinal depressions by a
195 prominent, sub-vertical lingual ridge that extends apicobasally. This ridge results from the
196 thickening of both dentine and enamel (Fig. 4B, C). A sub-circular boss (refer to lingual crown
197 buttress, sensu Wilson and Upchurch 2009) is developed on the distolingual surface; its surface is
198 smooth (Fig. 2C, D). This feature is widely distributed among mamenchisaurids and euhelopodids
199 (Suteethorn et al. 2013; Moore et al. 2020). Concerning the internal origin of this prominence, 3D
200 reconstruction based on micro-CT data provides evidence that the lingual boss arises from the
201 lingual expansion of the dentine, rather than from localized enamel thickening (Fig. 4F, G). In
202 contrast, the overlying enamel in this region is relatively uniform and thin in cross-section.

203
204 A distinct cingulum is present mesial to the boss on the lingual surface (Fig. 2C, D),
205 linguobasally extending from the crown's mesial margin. This feature is typical of *Euhelopus*
206 (Wilson and Upchurch 2009) and certain basal titanosauriforms (Zhang et al. 2024). Below this
207 cingulum, a mesiolingual surface is present (Fig. 2D, F). Apicodistal to the boss, a weak cingulum
208 is also observed. Below this, a distolingual facet (Fig. 2C, D) serves as an articular surface that
209 facilitates the imbricated arrangement of the teeth. This suggests that the distolingual surface of the
210 tooth overlapped the mesiolabial surface of the succeeding posterior tooth in life, a pattern noted
211 in *Mamenchisaurus sinocanadorum* (Moore et al. 2023).

212
213 **Root.** The preserved root measures 12.11 mm in height and is distinguished from the crown by
214 the cervix (Fig. 2C–H). It displays an oval cross-section (Fig. 2K, L). The mesial and distal margins

215 converge towards the midline as they extend apically, while the lingual margin converges towards
216 the labial side. Additionally, the dentine on the distal side of the root is thicker than that on the
217 mesial side.

218

219 **Enamel distribution.** Micro-CT data reveal the spatial distribution of enamel thickness (Figs 4,
220 5). In the apical half of the crown, enamel on the labial surface is significantly thicker than that on
221 the lingual surface (Figs 4B–D, 5A, 5C), regardless of enamel loss resulting from wear on the labial
222 surface. Conversely, enamel thickness becomes progressively more symmetrical towards the base
223 of the crown (Figs 4F–H, 5A, 5C). This pronounced labial thickening likely serves to reinforce the
224 crown against mechanical stress during shearing occlusion. Enamel thickness decreases basally on
225 both the labial and lingual sides. Three-dimensional analysis of enamel wall thickness (Fig. 5)
226 further characterizes this distribution within the observed regions. Notably, the labial surface (Fig.
227 5C) exhibits the most robust enamel distribution, with thickening (>0.56 mm) centrally located on
228 the apical half of the crown. In contrast, on the lingual surface (Fig. 5A), the maximum enamel
229 thickness (>0.56 mm) is confined exclusively to the lingual ridge. Additionally, the enamel is
230 largely lost on the mesial wear facet (Fig. 5B), while it becomes thinner at the distal wear facet
231 (Fig. 5D).

232

233 **Pulp cavity.** Three-dimensional reconstruction based on high-resolution micro-CT data (Fig. 6)
234 reveals that the pulp cavity is centrally positioned, with a total length exceeding 4.1 cm. The most
235 apical segment could not be reconstructed due to a fracture (Fig. 4B). Overall, the pulp cavity
236 exhibits a pronounced lingual curvature (Fig. 6B, D), corresponding to the recurvature observed in
237 the crown. The pulp cavity comprises both the root canal and the pulp chamber, with a distinct
238 morphological transition between these two anatomical components. The root canal represents the
239 most volumetrically extensive portion, characterized by an enlarged, bulbous morphology (Fig. 6A,
240 C), and its cross-section is approximately circular. The pulp chamber is a thin, laminar structure
241 that tapers apically. Its basal cross-section is slit-like (Fig. 4G), whereas the most apical cross-
242 section is small and circular (Fig. 4C).

243

244 Discussion

245 Relationships of PMOL-ADt0009

246

247 PMOL-ADt0009 is assigned to Eusauropoda based on a combination of characteristic features
248 of this clade, including the presence of a lingual concavity, V-shaped wear facet, wrinkled enamel
249 texture, a D-shaped mid-crown cross-section, a distolingual facet indicating overlapping tooth
250 crowns, and a labial groove (Upchurch 1998; Wilson and Sereno 1998; Wilson 2002; Upchurch et
251 al. 2004; Wilson 2005). Within Eusauropoda, PMOL-ADt0009 is excluded from Neosauropoda
252 because it retains marginal denticles, whose absence is generally regarded as a synapomorphy of
253 Neosauropoda (Wilson 2002; Upchurch et al. 2004). In non-neosauropod eusauropods, PMOL-
254 ADt0009 can be specifically referred to Mamenchisauridae, on the basis of the presence of
255 denticles along the mesial margin and their absence along the distal margin (Xing et al. 2015; Xu
256 et al. 2021).

257

258 In the Upper Jurassic of Xinjiang, mamenchisaurid fossils include five genera: *Xinjiangtitan*

259 (Wu et al. 2013), *Mamenchisaurus sinocanadorum* (Russell and Zheng 1993), *Tienshanosaurus*
260 (Young 1937), *Hudiesaurus* (Dong 1997), and *Rhomaleopakhus* (Upchurch et al. 2021). Of them,
261 only *M. sinocanadorum* has preserved teeth (Moore et al. 2020). PMOL-ADt0009 shows a parallel-
262 sided crown in labial or lingual view and a prominent boss at the lingual base, two distinctive
263 features of *M. sinocanadorum*. Nevertheless, it differs from *M. sinocanadorum* in retaining a
264 distinct labial longitudinal groove, whereas *M. sinocanadorum* has a convex, groove-less labial
265 surface (Moore et al. 2023). Additionally, *X. shanshanesis* has been shown to share a close
266 phylogenetic relationship with *M. sinocanadorum* (Moore et al. 2023), and may have similar dental
267 morphology. Given that PMOL-ADt0009 and *X. shanshanesis* were found in the same locality and
268 stratigraphic horizon, it is plausible that PMOL-ADt0009 may belong to *X. shanshanesis*.
269 Accordingly, we provisionally assign PMOL-ADt0009 to Mamenchisauridae *indet.* pending the
270 discovery of definitive dental material attributable to *X. shanshanesis*.

271
272 To date, aside from *Xinjiangtitan shanshanesis* (Wu et al. 2013; Zhang et al. 2020), the only
273 other reported sauropod fossil from the Qigu Formation is a putative mamenchisaurid tooth (SGP
274 2002/005) (Maisch and Matzke 2019a). PMOL-ADt0009 differs clearly from SGP 2002/005.
275 Specifically, PMOL-ADt0009 has a large crown measuring 34.1 mm in height, clearly defined
276 marginal denticles, a distinct distal labial groove, a prominent lingual boss, and wrinkled enamel
277 arranged in a sub-parallel pattern. In contrast, SGP 2002/005 features a smaller crown, measuring
278 17.8 mm in height, and lacks marginal denticles, a labial groove, and a distinct lingual boss, while
279 displaying an irregular anastomosing enamel pattern (Maisch and Matzke 2019a). Although the
280 presence of a lingual boss may vary depending on tooth position in *Mamenchisaurus*
281 *sinocanadorum* (Moore et al. 2023), the combination of these morphological differences likely
282 reflects true taxonomic diversity within the Qigu Formation rather than intraspecific variation. It
283 remains uncertain whether either specimen belongs to *Xinjiangtitan shanshanesis*, as no dental
284 material has been preserved for that taxon (Wu et al. 2013; Zhang et al. 2020). Collectively, these
285 dental morphological differences suggest the coexistence of at least two sauropod species within
286 the Qigu Formation.

287 288 *New dental anatomy of mamenchisaurids*

289
290 Research on mamenchisaurid teeth has primarily focused on their external morphology, as
291 demonstrated by previous studies (Pi et al. 1996; Russell and Zheng 1993; Zhang et al. 1998; Ye et
292 al. 2001; Ouyang and Ye 2002; Suteethorn et al. 2013; Averianov et al. 2019; Moore et al. 2023).
293 In contrast, the internal anatomy, including the histology of the lingual ridge and lingual boss, the
294 distribution of enamel thickness, and the three-dimensional structure of the pulp cavity, have
295 received little attention. This study aims to address this gap by using high-resolution non-
296 destructive Micro-CT imaging to provide the first comprehensive analysis of these internal features.

297
298 An apicobasal ridge within the lingual concavity is considered plesiomorphic for sauropods
299 (Upchurch 1998; Barrett et al. 2002), and is mainly found in clades characterized by broad,
300 spatulate crowns, such as Mamenchisauridae (Moore et al. 2023). This ridge may be homologous
301 with the mesiodistally convex lingual surface present on the crowns of numerous diplodocoids and
302 somphospondylans (Upchurch 1998; Upchurch et al. 2004). Despite the widespread presence of
303 this feature in sauropods, its histological structure remains poorly known. Analysis of high-

304 resolution micro-CT data from PMOL-ADt0009 reveals that the lingual ridge is formed by the
305 thickening of both enamel and dentine. Although the limited sample size precludes broad
306 generalisations, this observation provides direct evidence of the structural composition of the
307 lingual ridge and highlights the need for further histological investigations of sauropod teeth
308 exhibiting this feature.

309
310 A prominent distolingual boss has previously been considered a diagnostic feature of *Euhelopus*
311 (Wilson and Upchurch 2009). However, this morphological characteristic has also been reported in
312 *Mamenchisaurus* (Suteethorn et al. 2013; Moore et al. 2023) and in some isolated sauropod teeth
313 from the Late Jurassic to Early Cretaceous of China (Barrett & Wang, 2007; Amiot et al., 2010;
314 Upchurch et al. 2021; Zhang et al. 2024), Spain (Canudo et al. 2002), Thailand (Suteethorn et al.
315 2013), and Portugal (Mocho et al. 2017). Furthermore, the presence of this boss in *Yongjinglong*
316 remains uncertain (Li et al. 2014; Upchurch et al. 2021). Despite its taxonomic importance, the
317 internal structure of the boss has been poorly understood. Recent micro-CT studies by Zhang et al.
318 (2024) of a *Euhelopus*-like titanosauriform tooth from the Lower Cretaceous Yixian Formation
319 revealed that this feature results from an expansion of the dentine. Although the formation of the
320 boss in other lineages has yet to be verified, our cross-sectional analysis of PMOL-ADt0009
321 demonstrates that the boss in this mamenchisaurid tooth also forms through dentine thickening. This
322 finding supports the conclusion that the lingual boss is determined by dentine expansion and is
323 possibly homologous, at least in some mamenchisaurids and the *Euhelopus*-like titanosauriform
324 (Zhang et al. 2024).

325
326 Asymmetrical enamel thickness on the labial and lingual sides of tooth crowns is linked to
327 herbivory in large-bodied dinosaurs (D'Emic et al. 2013) and is an apomorphy within sauropods
328 (Sereno and Wilson 2005). Basal taxa like *Camarasaurus* show plesiomorphically uniform enamel
329 thickness around the tooth circumference (Sereno and Wilson 2005; D'Emic et al. 2013), whereas
330 neosauropod Diplodocoidea, such as *Nigersaurus* and *Diplodocus*, exhibit pronounced labiolingual
331 asymmetry (Sereno et al. 2007; D'Emic et al. 2013). Zhang et al. (2024) recently reported similar
332 enamel asymmetry in an early-diverging titanosauriform from the Yixian Formation, suggesting
333 this trait is likely more widespread among sauropods than previously recognized. Micro-CT data
334 reveal that PMOL-ADt0009, also shows distinct labiolingual enamel asymmetry, characterized by
335 thicker labial enamel. This pattern likely represents a convergent evolutionary event independent
336 of that observed in some eusauropod diplodocoids and titanosauriforms. Similar enamel asymmetry
337 has independently evolved in ornithischian clades such as Iguanodontia and Ceratopsia (Norman
338 2004; You and Dodson 2004; Zhang et al. 2024), but it has not been reported in herbivorous or
339 omnivorous theropods.

340
341 As far as we know, the three-dimensional geometry of the pulp cavity in mamenchisaurids has
342 remained undescribed until now. Using high-resolution micro-CT data, this study quantifies the
343 internal structure for the first time. The pulp cavity is centrally positioned and closely matches the
344 external crown profile. Along the apicobasal axis, the cavity shows a distinct volumetric change:
345 the basal root canal is large and bulbous, whereas apically it narrows sharply due to severe
346 labiolingual compression, transitioning rapidly into a lamina that appears as a slender, tapered sliver,
347 similar to the condition observed in a *Euhelopus*-like titanosauriform tooth (Zhang et al. 2024).
348 Furthermore, the combined volume of enamel and dentine volume is approximately 45 times

349 greater than that of the pulp cavity, confirming the tooth's solid composition and explaining its
350 mechanical strength.

351

352 **Conclusions**

353 This study reports a new isolated mamenchisaurid tooth (PMOL-ADt0009) from the Late Jurassic
354 Qigu Formation within the Turpan-Hami Basin. Morphological comparisons show that PMOL-
355 ADt0009 is a distinct morphotype, differing from the only known eusauropod tooth from the same
356 stratigraphic horizon. These differences suggest that sauropod diversity in the Qigu Formation has
357 been underestimated, indicating a more complex paleoecological landscape than previously
358 recognized. Additionally, this study provides the first three-dimensional reconstruction of
359 mamenchisaurid teeth, uncovering previously unknown internal structures. We show that the
360 lingual ridge forms from thickened enamel and dentine, the lingual boss is supported by substantial
361 dentine, and the pulp cavity shows a distinct "bulbous-to-laminar" transition. The identification of
362 labiolingual enamel asymmetry (labial > lingual) in the apical crown reveals a functional
363 convergence with derived neosauropods. Together, these findings highlight the importance of
364 internal tooth anatomy in understanding eusauropod evolution.

365

366 **Acknowledgement**

367 We thank Qiang Yang (Paleontological Museum of Liaoning, Shenyang) for his assistance in
368 tooth preparation, and Dr Shou-Ming Chen (Institute of Geology, Chinese Academy of Geological
369 Sciences, Beijing) for help with CT scanning.

370

371 **References**

372 Amiot R, Kusuhashi N, Xu X, Wang YQ (2010) Isolated dinosaur teeth from the Lower Cretaceous
373 Shahai and Fuxin formations of northeastern China. *Journal of Asian Earth Sciences* 39: 347–
374 358. <https://doi.org/10.1016/j.jseaes.2010.04.017>

375

376 Augustin FJ, Matzke AT, Maisch MW, Pfretzschner HU (2020) First evidence of an ankylosaur
377 (Dinosauria, Ornithischia) from the Jurassic Qigu Formation (Junggar Basin, NW China) and
378 the early fossil record of Ankylosauria. *Geobios* 61: 1–10.
379 <https://doi.org/10.1016/j.geobios.2020.06.005>.

380

381 Averianov A, Krasnolutskii S, Ivantsov S, Skutschas P, Schellhorn R, Schultz J, Martin T (2019)
382 Sauropod remains from the Middle Jurassic Itat Formation of West Siberia, Russia.
383 *Paläontologische Zeitschrift* 93: 691–701. <https://doi.org/10.1007/s12542-018-00445-8>

384

385 Barrett PM, Wang XL (2007) Basal titanosauriform (Dinosauria, Sauropoda) teeth from the Lower
386 Cretaceous Yixian Formation of Liaoning Province, China. *Palaeoworld* 16: 265–271.
387 <https://doi.org/10.1016/j.palwor.2007.07.001>

388

389 Barrett PM, Hasegawa Y, Manabe M, Isaji S, Matsuoka H (2002) Sauropod dinosaurs from the
390 Lower Cretaceous of eastern Asia: taxonomic and biogeographical implications.

- 391 Palaeontology 45: 1197–1217. <https://doi.org/10.1111/1475-4983.00282>
392
- 393 Bindellini G, Dal Sasso C (2021) Sauropod teeth from the Middle Jurassic of Madagascar, and the
394 oldest record of Titanosauriformes. *Papers in Palaeontology* 7: 137–161.
395 <https://doi.org/10.1002/spp2.1282>
396
- 397 Canudo JI, Ruiz-Omeñaca JI, Barco JL, Royo Torres R (2002) ¿Saurópodos asiáticos en el
398 Barremiense inferior (Cretácico Inferior) de España?. *Ameghiniana* 39: 443–452.
399 <https://www.ameghiniana.org.ar/index.php/ameghiniana/article/view/2689>
400
- 401 Dai H, Hu XF, Tan C, Ren XX, Ma QY, Wei GB, You HL (2025) A new mamenchisaurid sauropod
402 dinosaur from the upper jurassic of Southwest China reveals new evolutionary evidence from
403 East Asian eusauropods. *Scientific Reports* 15: 43308. [https://doi.org/10.1038/s41598-025-](https://doi.org/10.1038/s41598-025-29995-z)
404 [29995-z](https://doi.org/10.1038/s41598-025-29995-z)
405
- 406 D'Emic MD, Whitlock JA, Smith KM, Fisher DC, Wilson JA (2013) Evolution of High Tooth
407 Replacement Rates in Sauropod Dinosaurs. *PLOS ONE* 8: e69235.
408 <https://doi.org/10.1371/journal.pone.0069235>
409
- 410 Deng SH, Wang SE, Yang ZY, Lu YZ, Li X, Hu QY, An CZ, Xi DP, Wan XQ (2015) Comprehensive
411 study of the Middle-Upper Jurassic strata in the Junggar Basin, Xinjiang. *Acta Geoscientica*
412 *Sinica* 36: 559–574. <https://doi.org/10.3975/cagsb.2015.05.06>
413
- 414 Díez Díaz V, Tortosa T, Le Loeuff J (2013) Sauropod diversity in the Late Cretaceous of
415 southwestern Europe: The lessons of odontology. *Annales de Paléontologie* 99: 119–129.
416 <https://doi.org/10.1016/j.annpal.2012.12.002>
417
- 418 Dong ZM (1997) A gigantic sauropod (*Hudiesaurus sinojapanorum* gen. et sp. nov.) from the
419 Turpan Basin, China. In: Dong ZM (Ed.) *Sino-Japanese Silk Road Dinosaur Expedition*.
420 China Ocean Press, Beijing, 102–110.
421
- 422 He XL, Li K, Cai KJ (1988) The Middle Jurassic Dinosaur Fauna from Dashanpu, Zigong, Sichuan.
423 Vol. IV. Sauropod Dinosaurs (2): *Omeisaurus tianfuensis*. Sichuan Publishing House of
424 Science and Technology, Chengdu, 1–143pp.
425
- 426 Li LG, Li DQ, You HL, Dodson P (2014) A New Titanosaurian Sauropod from the Hekou Group
427 (Lower Cretaceous) of the Lanzhou-Minhe Basin, Gansu Province, China. *PLOS ONE* 9:
428 e85979. <https://doi.org/10.1371/journal.pone.0085979>
429
- 430 Li TJ, Huang ZL, Zhang YT, Wang R, Zhang H, Zhou ZH (2021) Lithofacies characteristics and
431 genetic model of shallow lacustrine fine- grained sediments and its geological significance for
432 shale oil in the Qiketai Formation in the Shengbei subsag, Turpan-Hami basin. *Acta Geologica*
433 *Sinica* 95: 3869–3884. <https://doi.org/10.19762/j.cnki.dizhixuebao.2021173>
434
- 435 Maisch MW, Matzke AT (2019a) First record of a eusauropod (Dinosauria: Sauropoda) from the

- 436 Upper Jurassic Qigu-Formation (southern Junggar Basin, China), and a reconsideration of
437 Late Jurassic sauropod diversity in Xinjiang. *Neues Jahrbuch für Geologie und Paläontologie*
438 - *Abhandlungen* 291: 109–117. <https://doi.org/10.1127/njgpa/2019/0792>
439
- 440 Maisch MW, Matzke AT (2019b) An isolated dinosaurian prootic with possible stegosaurian
441 affinities (Dinosauria: Thyreophora) from the Upper Jurassic Qigu Formation of the southern
442 Junggar Basin, NW-China. *Neues Jahrbuch für Geologie und Paläontologie - Abhandlungen*
443 294: 275–283. <https://doi.org/10.1127/njgpa/2019/0859>
444
- 445 Maisch MW, Matzke AT (2020) Small theropod teeth (Dinosauria) from the Upper Jurassic Qigu
446 Formation of the southern Junggar Basin, NW China. *Neues Jahrbuch für Geologie und*
447 *Paläontologie – Abhandlungen* 295: 91–100. <https://doi.org/10.1127/njgpa/2020/0869>
448
- 449 Mannion PD, Upchurch P, Schwarz D, Wings O (2019) Taxonomic affinities of the putative
450 titanosaurs from the Late Jurassic Tendaguru Formation of Tanzania: phylogenetic and
451 biogeographic implications for eusauropod dinosaur evolution. *Zoological Journal of the*
452 *Linnean Society* 185: 784–909. <https://doi.org/10.1093/zoolinnean/zly068>
453
- 454 Martin T, Averianov AO, Pfretzschner HU (2010a) Mammals from the Late Jurassic Qigu
455 Formation in the Southern Junggar Basin, Xinjiang, Northwest China. *Palaeobiodiversity and*
456 *Palaeoenvironments* 90: 295–319. <https://doi.org/10.1007/s12549-010-0030-4>
457
- 458 Martin T, Sun G, Mosbrugger V (2010b) Triassic-Jurassic biodiversity, ecosystems, and climate in
459 the Junggar Basin, Xinjiang, Northwest China. *Palaeobiodiversity and Palaeoenvironments*
460 90: 171–173. <https://doi.org/10.1007/s12549-010-0035-z>
461
- 462 Matzke AT, Maisch MW, Sun G, Pfretzschner HU, Stöhr H (2005) A New Middle Jurassic
463 Xinjiangchelyid Turtle (Testudines; Eucryptodira) from China (Xinjiang, Junggar Basin).
464 *Journal of Vertebrate Paleontology* 25: 63–70. <http://www.jstor.org/stable/4524417>
465
- 466 Mocho P, Royo-Torres R, Malafaia E, Escaso F, Ortega F (2017) Sauropod tooth morphotypes from
467 the Upper Jurassic of the Lusitanian Basin (Portugal). *Papers in Palaeontology* 3: 259–295.
468 <https://doi.org/10.1002/spp2.1075>
469
- 470 Moore AJ, Upchurch P, Barrett PM, Clark JM, Xu X (2020) Osteology of *Klamelisaurus gobiensis*
471 (Dinosauria, Eusauropoda) and the evolutionary history of Middle-Late Jurassic Chinese
472 sauropods. *Journal of Systematic Palaeontology* 18: 1299–1393.
473 <https://doi.org/10.1080/14772019.2020.1759706>
474
- 475 Moore AJ, Barrett PM, Upchurch P, Liao CC, Ye Y, Hao BQ, Xu X (2023) Re-assessment of the
476 Late Jurassic eusauropod *Mamenchisaurus sinocanadorum* Russell and Zheng, 1993, and the
477 evolution of exceptionally long necks in mamenchisaurids. *Journal of Systematic*
478 *Palaeontology* 21: 2171818. <https://doi.org/10.1080/14772019.2023.2171818>
479
- 480 Norman DB (2004) Basal Iguanodontia. In: Weishampel DB, Dodson P, Osmólska H (Eds) *The*

- 481 Dinosauria, Second Edition. University of California Press, Berkeley, 413–437.
482 https://archive.org/details/epdf.pub_the-dinosauria-2nd-edition/mode/1up
483
- 484 Ouyang H, Ye Y (2002) The First Mamenchisaurian Skeleton with Complete Skull,
485 *Mamenchisaurus youngi*. Sichuan Publishing House of Science and Technology, Chengdu,
486 111pp.
487
- 488 Pfitzschner HU, Martin T, Maisch MW, Matzke AT, Sun G (2005) A new docodont mammal from
489 the Late Jurassic of the Junggar Basin in Northwest China. *Acta Palaeontologica Polonica* 50:
490 799–808. <https://app.pan.pl/archive/published/app50/app50-799.pdf>
491
- 492 Pi LZ, Ouyang H, Ye Y (1996) A new species of sauropod from Sichuan Basin, *Mamenchisaurus*
493 *youngi*. In: Editorial Committee (Eds) Papers on Geosciences Contributed to the 30th
494 International Geological Congress. 30th International Geological Congress, Beijing (China),
495 August 1996. Chengdu University of Science and Technology Press, Chengdu, 87–91.
496
- 497 Rabi M, Zhou CF, Wings O, Sun G, Joyce WG (2013) A new xinjiangchelyid turtle from the Middle
498 Jurassic of Xinjiang, China and the evolution of the basiptyergoid process in Mesozoic turtles.
499 *BMC Evolutionary Biology* 13: 203. <https://doi.org/10.1186/1471-2148-13-203>
500
- 501 Ren XX, Huang JD, You HL (2020) The second mamenchisaurid dinosaur from the Middle Jurassic
502 of Eastern China. *Historical Biology* 32: 602–610.
503 <https://doi.org/10.1080/08912963.2018.1515935>.
504
- 505 Ren XX, Sekiya T, Wang T, Yang ZW, You HL (2021) A revision of the referred specimen of
506 *Chuanjiesaurus anaensis* Fang et al., 2000: a new early branching mamenchisaurid sauropod
507 from the Middle Jurassic of China. *Historical Biology* 33: 1872–1887.
508 <https://doi.org/10.1080/08912963.2020.1747450>.
509
- 510 Ren XX, Wang XR, Ji YN, Guo Z, Ji Q (2025) The first mamenchisaurid from the Upper Jurassic
511 Dongxing Formation of Guangxi, southernmost China. *Historical Biology* 37: 465–478.
512 <https://doi.org/10.1080/08912963.2024.2309287>
513
- 514 Russell DA, Zheng Z (1993) A large mamenchisaurid from the Junggar Basin, Xinjiang, People's
515 Republic of China. *Canadian Journal of Earth Sciences* 30: 2082–2095.
516 <https://doi.org/10.1139/e93-180>
517
- 518 Sereno PC, Wilson JA (2005) Structure and Evolution of a Sauropod Tooth Battery. In: Curry
519 Rogers KA, Wilson JA (Eds) *The Sauropods: Evolution and Paleobiology*. University of
520 California Press, Berkeley, 157–177.
521 <https://doi.org/10.1525/california/9780520246232.003.0006>
522
- 523 Sereno PC, Wilson JA, Witmer LM, Whitlock JA, Maga A, Ide O, Rowe TA (2007) Structural
524 Extremes in a Cretaceous Dinosaur. *PLOS ONE* 2: e1230.
525 <https://doi.org/10.1371/journal.pone.0001230>

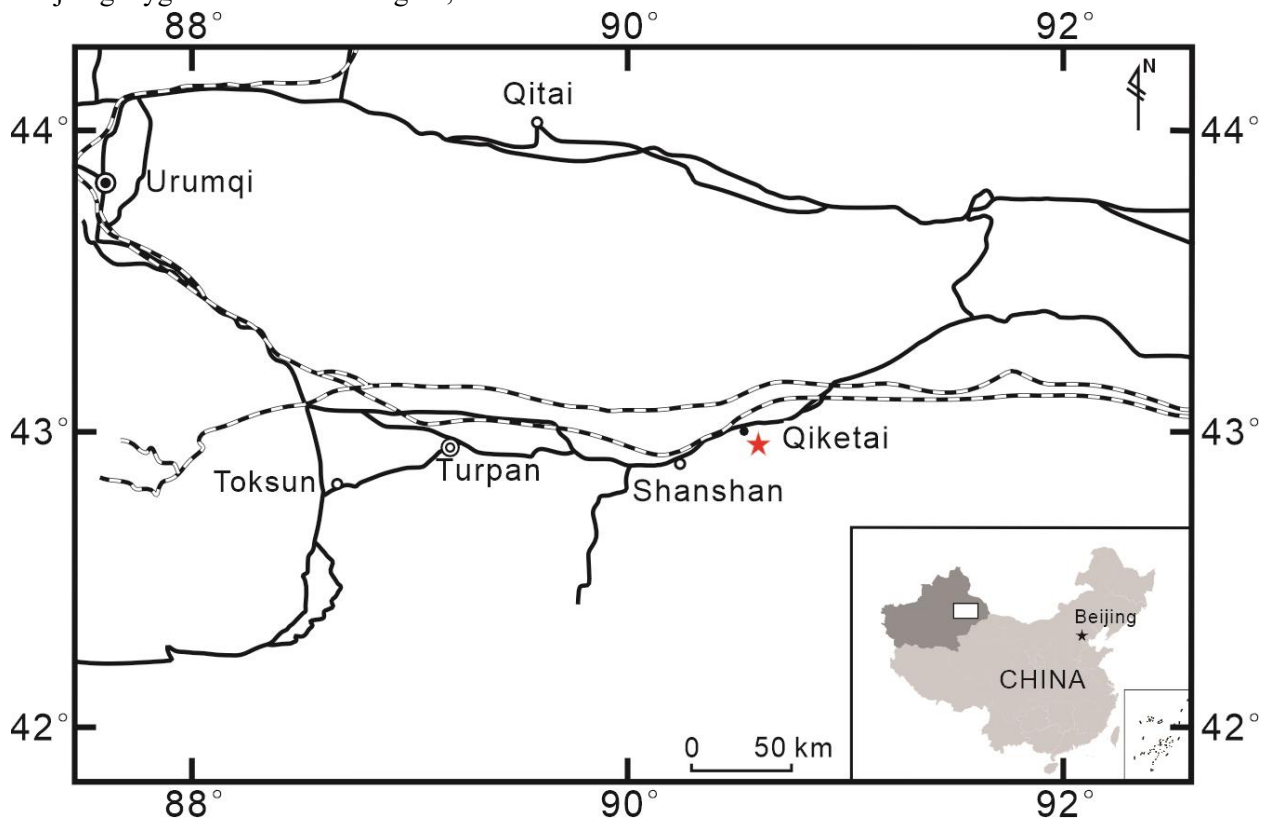
- 526
527 Song ZR, Cao SH, Wang Z, Wang SH, Wang B, Xu LS (2014) Geological Heritage Survey and
528 Evaluation Report of Shanshan County, Xinjiang. Jiangxi Geological Survey Institute,
529 Nanchang-Jiangxi Province, 19–101.
530
- 531 Suteethorn S, Le Loeuff J, Buffetaut E, Suteethorn V, Wongko K (2013) First evidence of a
532 mamenchisaurid dinosaur from the Upper Jurassic-Lower Cretaceous Phu Kradung Formation
533 of Thailand. *Acta Palaeontologica Polonica* 58: 459–469.
534 <https://doi.org/10.4202/app.2009.0155>
535
- 536 Upchurch P (1998) The phylogenetic relationships of sauropod dinosaurs. *Zoological Journal of*
537 *the Linnean Society* 124: 43–103. <https://doi.org/10.1111/j.1096-3642.1998.tb00569.x>
538
- 539 Upchurch P, Barrett PM, Dodson P (2004) Sauropoda. In: Weishampel DB, Dodson P, Osmólska
540 H (Eds) *The Dinosauria, Second Edition*. University of California Press, Berkeley, 259–322.
541 https://archive.org/details/epdf.pub_the-dinosauria-2nd-edition/mode/1up
542
- 543 Upchurch P, Mannion PD, Xu X, Barrett PM (2021) Re-assessment of the Late Jurassic eusauropod
544 dinosaur *Hudiesaurus sinojapanorum* Dong, 1997, from the Turpan Basin, China, and the
545 evolution of hyper-robust antebrachia in sauropods. *Journal of Vertebrate Paleontology* 41:
546 e1994414. <https://doi.org/10.1080/02724634.2021.1994414>
547
- 548 Wei XF, Tan YJ, Jiang S, Ding J, Li L, Wang XB, Liu YY, Wei GB, Li DL, Liu Y, Peng GZ, Zhang
549 SZ, Lao CL (2025) A new mamenchisaurid from the Upper Jurassic Suining Formation of the
550 Sichuan Basin in China and its implication on sauropod gigantism. *Scientific Reports* 15:
551 24808. <https://doi.org/10.1038/s41598-025-09796-0>
552
- 553 Wilson JA (2002) Sauropod dinosaur phylogeny: critique and cladistic analysis. *Zoological Journal*
554 *of the Linnean Society* 136: 215–275. <https://doi.org/10.1046/j.1096-3642.2002.00029.x>
555
- 556 Wilson JA (2005) Overview of Sauropod Phylogeny and Evolution. In: Rogers KC, Wilson JA (Eds)
557 *The Sauropods: Evolution and Paleobiology*. University of California Press, Berkeley, 15–49.
558
- 559 Wilson JA, Sereno PC (1998) Early Evolution and Higher-Level Phylogeny of Sauropod Dinosaurs.
560 *Journal of Vertebrate Paleontology* 18: 1–79.
561 <https://doi.org/10.1080/02724634.1998.10011115>
562
- 563 Wilson JA, Upchurch P (2009) Redescription and reassessment of the phylogenetic affinities of
564 *Euhelopus zdanskyi* (Dinosauria: Sauropoda) from the Early Cretaceous of China. *Journal of*
565 *Systematic Palaeontology* 7: 199–239. <https://doi.org/10.1017/S1477201908002691>
566
- 567 Wings O, Pfretzschner HU, Maisch MW (2007) The first evidence of a stegosaur (Dinosauria,
568 Ornithischia) from the Jurassic of Xinjiang/China. *Neues Jahrbuch für Geologie und*
569 *Paläontologie - Abhandlungen* 243: 113–118. [https://doi.org/10.1127/0077-7749/2007/0243-](https://doi.org/10.1127/0077-7749/2007/0243-0113)
570 [0113](https://doi.org/10.1127/0077-7749/2007/0243-0113).

- 571
572 Wings O, Tütken T, Fowler DW, Martin T, Pfretzschner HU, Sun G (2015) Dinosaur teeth from the
573 Jurassic Qigu and Shishugou Formations of the Junggar Basin (Xinjiang/China) and their
574 paleoecologic implications. *Paläontologische Zeitschrift* 89: 485–502.
575 <https://doi.org/10.1007/s12542-014-0227-3>
576
- 577 Wings O, Rabi M, Schneider JW, Schwermann L, Sun G, Zhou CF, Joyce WG (2012) An enormous
578 Jurassic turtle bone bed from the Turpan Basin of Xinjiang, China. *Naturwissenschaften* 99:
579 925–935. <https://doi.org/10.1007/s00114-012-0974-5>
580
- 581 Wu WH, Zhou CF, Wings O, Sekiya T, Dong ZM (2013) A new gigantic sauropod dinosaur from
582 the Middle Jurassic of Shanshan, Xinjiang. *Global Geology* 32: 437–446.
583
- 584 XBGMR (Xinjiang Bureau of Geology and Mineral Resources) (1993) *Regional Geology of*
585 *Xinjiang Uygur Autonomous Region*. Geological Publishing House, Beijing, 207–266.
586
- 587 Xing LX, Miyashita T, Zhang JP, Li DQ, Ye Y, Sekiya T, Wang FP, Currie PJ (2015) A new sauropod
588 dinosaur from the Late Jurassic of China and the diversity, distribution, and relationships of
589 mamenchisaurids. *Journal of Vertebrate Paleontology* 35: e889701.
590 <https://doi.org/10.1080/02724634.2014.889701>
591
- 592 Xu X, You HL, Mo JY (2021) Amphibians, reptilians and avians: Saurischian dinosaurs. In: Li JL,
593 Zhou ZH (Eds) *Palaeovertebrata Sinica*, Volume 2. Science Press, Beijing, 1–375.
594
- 595 Ye Y, Ouyang H, Fu QM (2001) New material of *Mamenchisaurus hochuanensis* from Zigong,
596 Sichuan. *Vertebrata Palasiatica* 39: 266–271.
597
- 598 You HL, Dodson P (2004) Basal Ceratopsia. In: Weishampel DB, Dodson P, Osmólska H (Eds)
599 *The Dinosauria*, Second Edition. University of California Press, Berkeley, 478–493.
600 https://archive.org/details/epdf.pub_the-dinosauria-2nd-edition/mode/1up
601
- 602 Young CC (1937) A new dinosaurian from Sinkiang. *Palaeontologia Sinica*, New Series C 2: 1–25.
603
- 604 Young CC (1954) On a new sauropod from Yiping, Szechuan, China. *Acta Palaeontologica Sinica*
605 2: 355–369.
606
- 607 Zhang HG, Yin YL, Pei R, Zhou CF (2024) Early-diverging Titanosauriform (Dinosauria,
608 Sauropoda) Teeth from the Lower Cretaceous Yixian Formation of Southeastern Inner
609 Mongolia, Northeast China. *Acta Geologica Sinica (English Edition)* 98: 303–310.
610 <https://doi.org/10.1111/1755-6724.15169>
611
- 612 Zhang XQ, Li DQ, Xie Y, You HL (2020) Redescription of the cervical vertebrae of the
613 Mamenchisaurid Sauropod *Xinjiangtitan shanshanensis* Wu et al. 2013. *Historical Biology* 32:
614 803–822. <https://doi.org/10.1080/08912963.2018.1539970>
615

616 Zhang YH, Li K, Zeng QH (1998) A new species of sauropod dinosaur from the upper Jurassic of
617 Sichuan Basin, China. *Journal of Chengdu University of Technology* 25: 61–70.
618

619 **Figure captions**

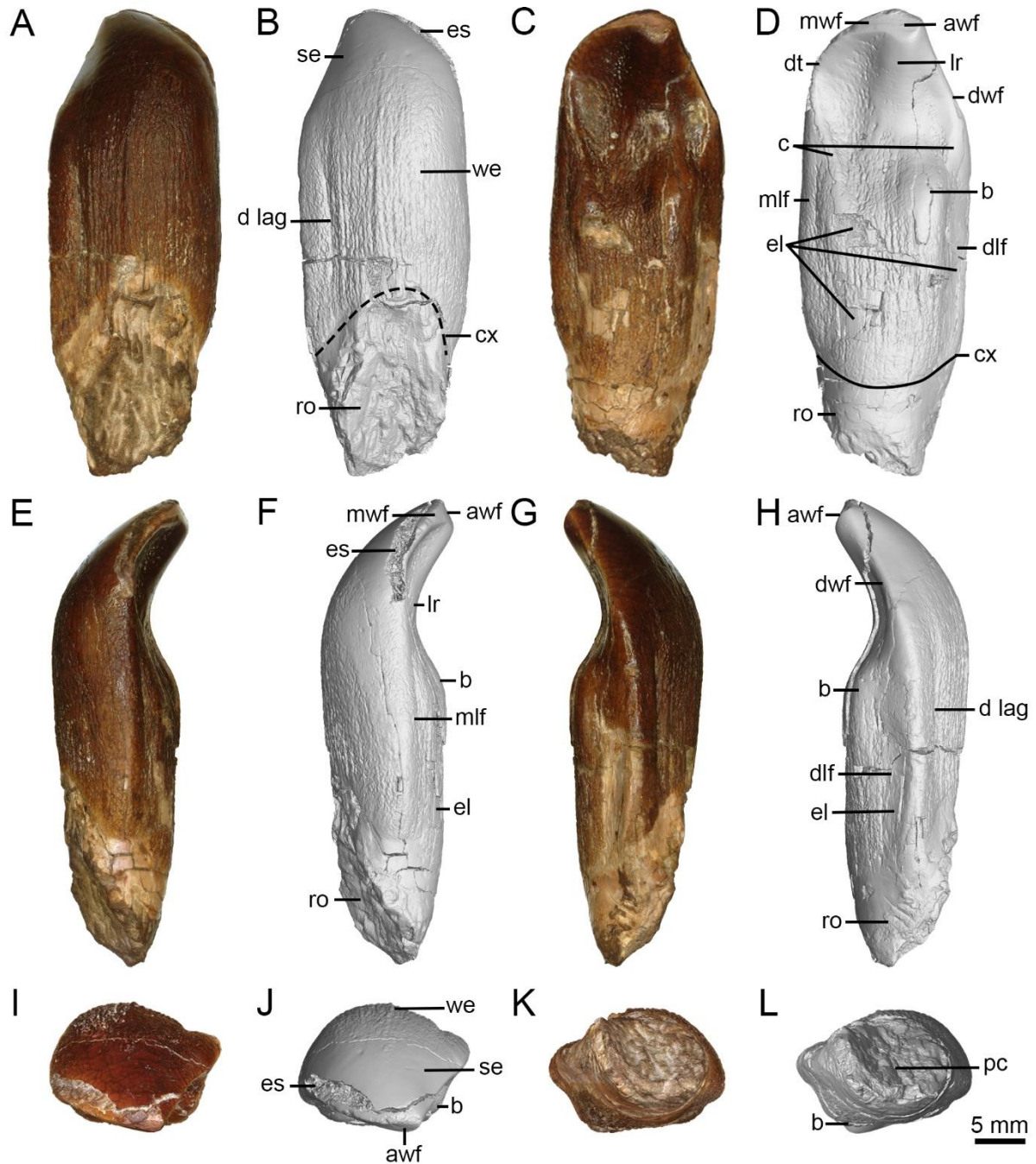
620 **Figure 1.** Geographic position of fossil locality (marked by a red star) in Qiketai Town, Shanshan County,
621 Xinjiang Uygur Autonomous Region, China.



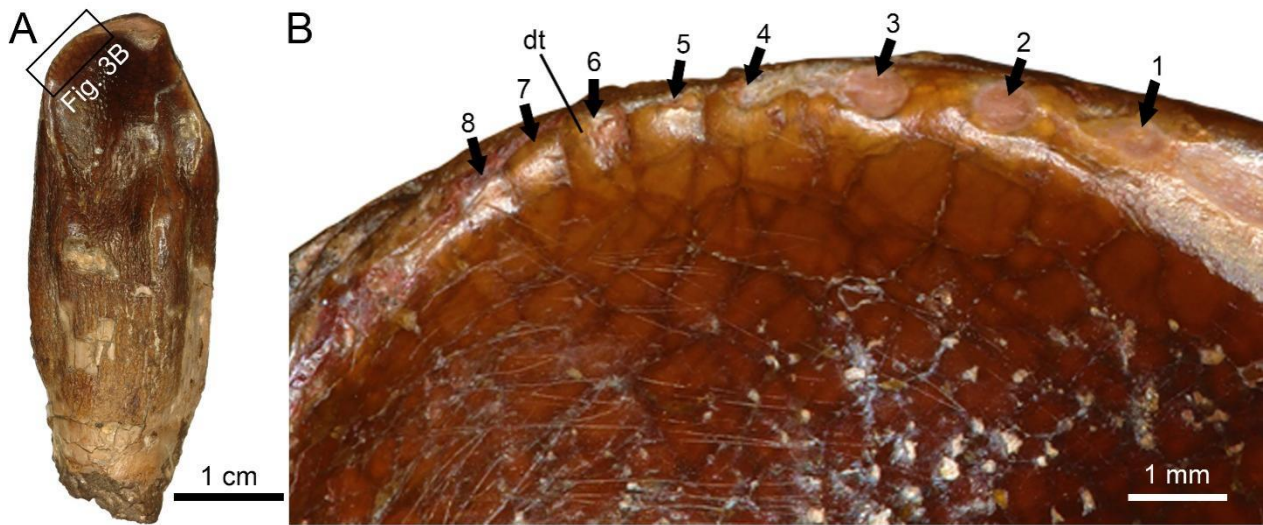
622

623

624 **Figure 2.** Mamenchisaurid tooth (PMOL-ADt0009) in labial (A, B), lingual (C, D), mesial (E, F), distal (G, H), apical (I, J) and basal (K, L) views. Abbreviations: awf, apical wear facet; b, boss; c, cingulum; lr, lingual ridge; cx, cervix; dt, denticle; d lag, distal labial groove; dlf, distolingual facet; dwf, distal wear facet; es, enamel spalling; mlf, mesiolingual facet; mwf, mesial wear facet; pc, pulp cavity; ro, root; se, smooth enamel; we, wrinkled enamel.



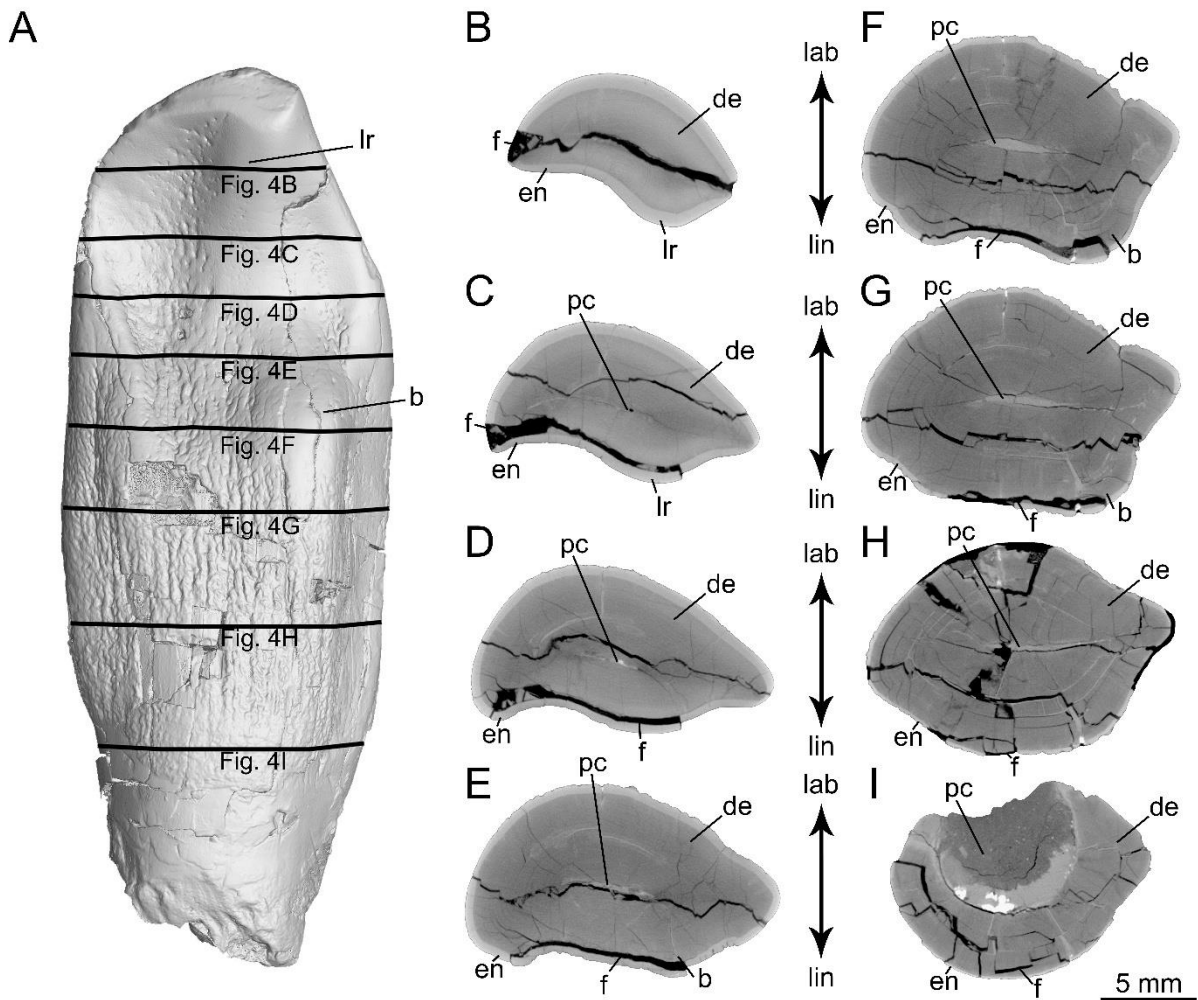
631 **Figure 3.** Mamenchisaurid tooth (PMOL-ADt0009). **A.** In lingual view; **B.** Detailed view of the mesial
632 marginal denticles with numbers 1–8 indicating individual denticles. Abbreviations: dt, denticle.



633

634

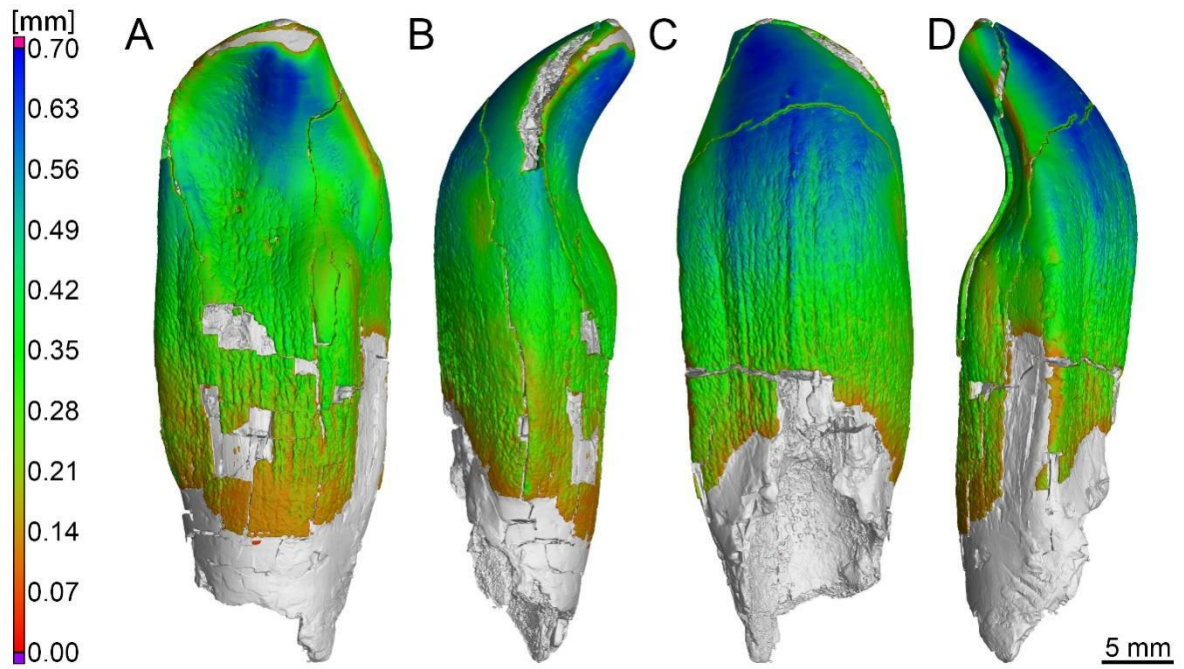
635 **Figure 4.** CT rendered images of the mamenchisaurid tooth (PMOL-ADt0009). **A.** Tooth in lingual view
636 with selected cross-sections (**B–I**). Abbreviations: b, boss; de, dentine; en, enamel; f, fissure/fracture; lab,
637 labial; lin, lingual; lr, lingual ridge; pc, pulp cavity.



638

639

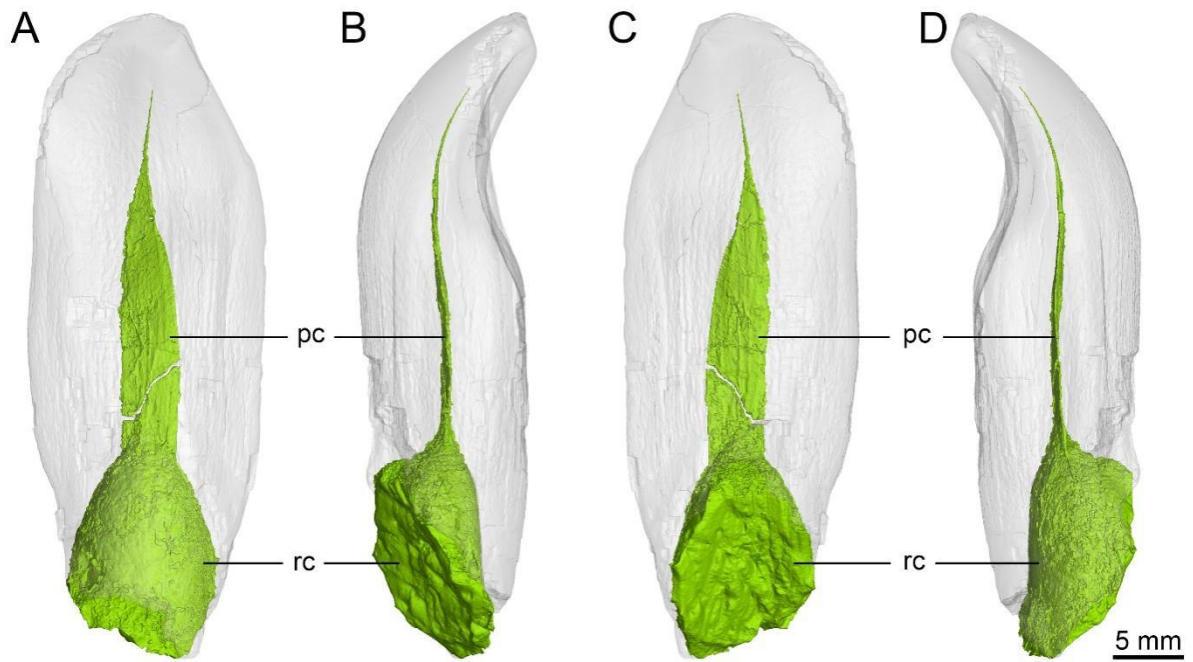
640 **Figure 5.** Three-dimensional analysis of enamel wall thickness in the mamenchisaurid tooth (PMOL-
641 ADt0009) in lingual (**A**), mesial (**B**), labial (**C**), and distal (**D**) views.



642

643

644 **Figure 6.** Semi-transparent CT rendered images of the mamenchisaurid tooth (PMOL-ADt0009) with pulp
645 cavity highlighted in lingual (A), mesial (B), labial (C), and distal (D) views. Abbreviations: rc, root canal;
646 pc, pulp chamber.



647
648

649 **Table 1.** Morphometric (in mm) data of mamenchisaurid tooth (PMOL-ADt0009).
 650

Items	PMOL-ADt0009
Total length	46.21
Crown height	34.10
Maximum mesiodistal crown length	16.78
Maximum labiolingual crown width	13.02
Root height	12.11
Mesiodistal width of tooth crown at its base	14.32
Slenderness index	2.03
Compression index	0.80
Expansion index	1.17

651